Resonant-state-induced interference minima in high-order harmonic generation from liquid systems

Ai-Yuan He(贺爱源)[1], Guang-Xian Xiao(肖广贤)[1], Nian-Zhuo Mai(买年卓)[1] and Chang-Long Xia(夏昌龙)[1] *

[1]College of Physics and Electronic Engineering, Shanxi Normal University, Taiyuan 030031, China

September 15, 2026

Abstract

High-order harmonic generation (HHG) from liquid systems is investigated by a random atomic chain model. It is found that the interference minimum appears in the harmonic spectrum, and the position of the spectral minimum increases monotonically with increasing laser wavelength in the range of [1300, 1700] nm. The paths contributing to the harmonics have been defined to explain the cause of the harmonic minimum. For the case of laser wavelength in the range of $[1300, 1600]$ nm, the harmonic minimum results from the interference cancellation between path IA and path IB. For the case of a longer wavelength, such as 1700 nm, the harmonic minimum is produced by the interference cancellation between path I and path II. It is stated that lasers with longer wavelengths have a higher probability of driving electrons to more distant areas, and path II plays a crucial role in harmonic radiation. Time-dependent population of quasi-free states and the time-dependent evolution of electrons in the coordinate space are also simulated to analyze the physical processes. A new perspective for understanding the source of harmonic order interference cancellation is provided, and this might be used for further research on the mechanism of liquid harmonic radiation.

Keywords: Liquid harmonic generation, Interference minimum, Localized resonant states

PACS: 42.50.Hz, 42.65.Ky, 78.47.N-

1. Introduction

High-order harmonic generation (HHG) is a striking extreme nonlinear optical phenomenon in strong-field physics. It features a classic plateau structure that serves as an effective source for attosecond pulse generation [1,2], providing a tool for probing matter at the atomic scale. HHG in gas [3,4], crystals [5,6], plasma [7,8] and quasicrystals [9–12] has been discussed and examined in many works. Theoretical advances have been propelled by the three-step model [13], interband and intraband mechanisms [14], and semiclassical trajectory approaches [15]. Recently, liquids, as a common state of matter, have also attracted considerable attention in the context of HHG. The perturbative-regime harmonics have been observed in early works [16–20]. While these results are limited by the experimental setup thereby impossible to separate the harmonics generated

*Corresponding author. E-mail: xiachl2008@163.com

by the liquid molecules from those generated by the surrounding gaseous molecules. Until 2018, T. T. Luu *et al.* [21] extracted successfully pure liquid harmonics by liquid flat-microjet technology, which suggests this area holds potential for further development.

The liquid systems exhibit short-range order and long-range disorder, which can be verified through X-ray diffraction (XRD) analysis. A disordered atomic chain model was proposed to study the HHG from liquid systems [22]. In this model, the radial distribution function can be obtained by statistically analyzing the distances between atomic pairs, see in Fig. S1 of the *Supplementary Materials*. And it has been confirmed to be consistent with the experimental results [22,23], thereby confirming the rationality of the model. The cutoff energy in HHG from liquids is linearly correlated with the E_0 of the field [22,24], while showing no dependence on wavelength [25]. An ab initio cluster-based approach has also been developed to describe bulk liquids [26], which reveals the unique nonlinear nature in liquids. Furthermore, information about microscopic structure can also be explored from liquid HHG. For example, a statistical two-level resonance model based on wave functions that incorporate the localized resonant states in liquids was proposed to explain why the harmonic cutoff cannot be significantly broadened under a two-color scheme [27]. Recently, the discovery of multi-plateau structure revealed the mechanism of off-site recombination in liquids [28]. Research on liquids HHG has made breakthrough [29–32], while research on the harmonic interference structures is quite scarce.

Harmonic interference structure is one of the essential parameters for analyzing the ultrafast processes in matters. In molecular HHG, spectral minima are commonly associated with structural interference, where the emitted harmonics from different atomic centers or molecular orbitals interfere due to the spatial distribution and symmetry of the molecular wave functions [33,34]. In gas-phase HHG, interference effects are mainly related to different electron trajectories, such as the interference between short and long trajectories [35] within the three-step model [13]. The interference features observed in crystals are determined by their band structure, including interband interference [36], interference between different crystal momentum channels [37,38] and trajectory interference in momentum space [39]. In the emerging field of liquid HHG, a phenomenon of minima in the liquid harmonic spectrum also appears in many investigations [21,22,24,26,27], but as far as we know, this has not been thoroughly discussed. The liquid systems have wave functions with localized resonant states, which are characterized by two initial states occupying the same spatial position [27]. This characteristic inevitably endows liquid systems with electronic transition and recombination mechanisms that are distinct from those of gas-phase HHG and solid-state HHG. However, the interference analysis method based on crystal momentum is difficult to be directly applied to liquid systems lacking long-range periodic structures. Therefore, identifying how these localized states participate in harmonic emission and how their phase relationship affects the harmonic spectrum remains an unresolved fundamental question.

In this paper, a one-dimensional disordered model is employed, and the electron transition mechanisms encoded in the spectra minimum is analyzed by numerically solving the time-dependent Schrödinger equation (TDSE). The simulation results show that interference minimum in the harmonic spectrum tend to appear in liquid systems. The interference of different paths occurs when electrons that have been ionized from the nucleus to quasi-free states undergo interband transitions. Given the characteristic of localized resonant states in the liquid systems, our interpretation is to explain the phenomenon of the spectral minimum by separating the harmonic radiation sources. The different transition trajectories, namely path IA, path IB, and path II

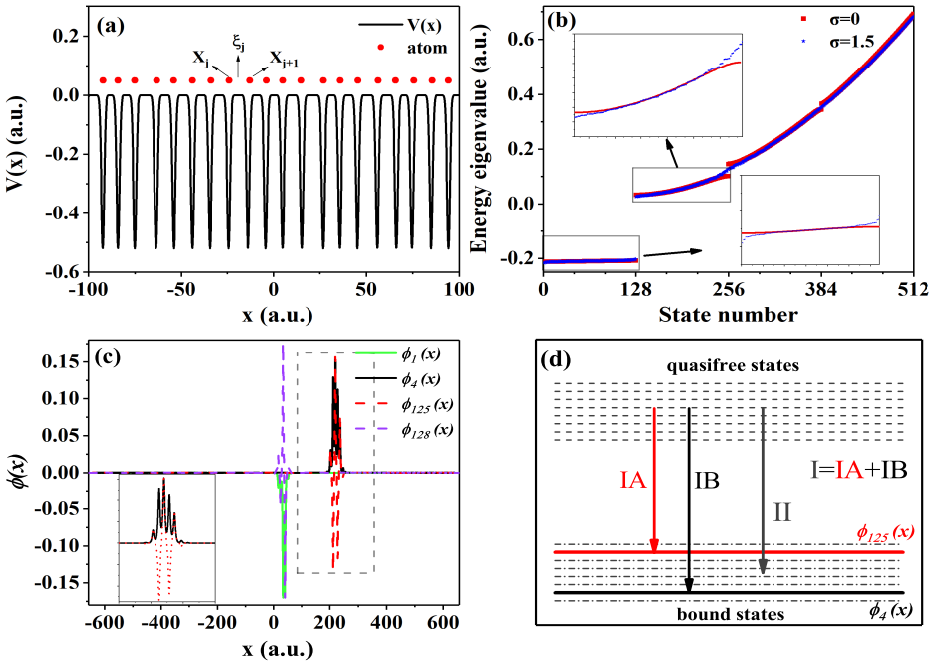


Fig. 1. (a) The schematic diagram of the potential function for the one-dimensional disorder model of liquid systems. (b) The energy band structures for the case of $\sigma = 0$ and 1.5. The insets at the bottom right corner and the top left corner are enlarged views of eigenenergy for bound states and quasi-free states. (c) The wave function of bound states for the case of $\sigma = 1.5$. The inset at the bottom left corner is an enlarged view of $\phi_4(x)$ and $\phi_{125}(x)$.(d) Schematic diagram of the excited electrons returning to the initial state (IA),the corresponding resonant state(IB) and other states (II).

are defined, which correspond to the paths of initial state-combination, resonance state-combination, and other state-combination. The sum of the contributions of path IA and path IB is denoted as path I, which stands for the electron after transitioning to the spatial position of the initial state. By altering the wavelength of the incident laser, the applicability range of the physical mechanism is investigated. The time-dependent population imaging (TDPI) of quasi-free states is also simulated to resolve the electron dynamic processes.

2. The disorder model and theoretical method

One-dimensional disorder atomic chain is employed in this study [22,27], and the schematic diagram of the potential function is shown in Fig. 1(a), the red circles denote liquid atoms, and the distance between the two adjacent cores is a set of random numbers and satisfies the one-dimensional normal distribution, *i.e.,* $f(\xi) = \frac{1}{\sqrt{2\pi\sigma^2}} \exp[-\frac{(\xi-a)^2}{2\sigma^2}]$. The degree of disorder is described by the standard deviation σ. The potential function between the cores X_j and X_{j+1} can be expressed as:

$$V(x) = -V_0 \left\{ \exp[-\frac{(x-X_j)^2}{2\alpha^2}] + \exp[-\frac{(x-X_{j+1})^2}{2\alpha^2}] \right\}, \tag{1}$$

where $V_0 = 0.52$ *a.u.* determine the depth of the potential function, $\alpha = 0.08a_0$ controls the width and $a_0 = 10$ *a.u.* is the average atomic spacing. It is necessary to use a truncated normal distribution to simulate the randomness of liquid atoms and the truncated range is set as an interval $[\frac{2}{3}a_0, \frac{4}{3}a_0]$. In the simulation, we excluded the configurations whose average value and standard deviation exceed 0.05. For further discussion,

please refer to Fig. S2 of the *Supplementary Materials*. The black solid line in Fig. 1(a) is a schematic diagram of the potential wells, and all potential wells are arranged at random distances. Although this model neglects the internal structure of liquid molecules, it can still effectively describe the randomness and short-range order of liquids. And it is useful to analyze the physical mechanism of liquid harmonic radiation. The cutoff of the liquid harmonics predicted by this model is independent of the laser wavelength [22], and this has been verified in subsequent experiments [25]. This demonstrates the validity and reliability of this model.

The eigenstates and eigenvalues are obtained by solving the stationary Schrödinger equation, $\hat{H}\phi_n(x) = E_n\phi_n(x)$. As shown in Fig. 1(b), there is a band gap between E_{128} and E_{129} and the states below the band gap are bound states, while the states above the band gap are quasi-free states. The state number corresponding to each band is 128 because the number of nuclei in the random chain is $N = 128$ in our simulation. The energy band for the case of the periodic system ($\sigma = 0$) is also simulated for comparison. The insets in the lower right corner and upper left corner are enlarged views of eigenenergy for bound states and quasi-free states, respectively, reflecting the feature that the energy bands of the liquid systems are less smooth compared with those of the periodic system. Fig. 1(c) presents four representative wave functions chosen to exemplify the significant spatial locality observed, for the cases of $\phi_1(x)$, $\phi_4(x)$, $\phi_{125}(x)$, and $\phi_{128}(x)$, respectively. In liquid systems, with the mid-gap states of the bound states as the center, the wave functions at the two corresponding ends form mutual resonant states, which have been discussed in Ref. [27]. Therefore, the initial state $\phi_n(x)$ and $\phi_{N-n+1}(x)$ are each a pair of mutually resonant states, which peaks basically coincident after the modulus squared. The wave functions of the pair of mutually resonant states on the bound states have different symmetries, *e.g.*, the state $\phi_4(x)$ is a completely positive wave function, while the corresponding resonant state $\phi_{125}(x)$ has both positive and negative values. When a laser is introduced, the electron population can transfer between the resonant states in response to the oscillation of the laser pulse. The inconsistency in the symmetry of the resonance states will affect the process of harmonic radiation. Due to the resonant local characteristics of the eigenstates in liquid systems, the paths leading to the harmonic bands can be classified into path IA, path IB and path II, as shown in Fig. 1(d). The pathways for electrons excited to the quasi-free state returning to the initial state $\phi_n(x)$ and the corresponding resonant state $\phi_{N-n+1}(x)$ are defined as path IA and path IB, respectively, whereas those returning to other bound states are classified as path II. The total contribution of path IA and path IB is defined as path I. The harmonics contributed by different paths carry different phases, and the total harmonic is the combined contribution of these paths.

The TDSE under the influence of the laser field is solved by selecting each bound state in the disordered chain model as the initial state. TDSE can be written as (atomic units are used in this paper, *i.e., a.u.*):

$$i\frac{\partial\psi(x,t)}{\partial t} = [-\frac{\partial^2}{2\partial x^2} + V(x) + xE(t)]\psi(x,t). \tag{2}$$

Where $E(t)$ is the two-color synthesized laser field and can be expressed as

$$E\left(t\right) = f\left(t\right)\left[E_1 cos(\omega_1 t) + E_2 cos(\omega_2 t)\right], \tag{3}$$

$E_1 = 0.012$ *a.u.* denotes the electric field strength of the fundamental field and corresponds to the intensity $I_1 = 5.05 \times 10^{12} W/cm^2$. For the fundamental field, the wavelength is $\lambda_1 = 1600$ *nm*. For the second laser pulse, the electric field amplitude and frequency are denoted as $E_2 = 0.3E_1$ and $\omega_2 = 3\omega_1$, respectively. $f(t)$ is trapezoidal envelope with eight optic cycles. In the simulation, the number of spatial grid points is 8192, with

a corresponding step size of approximately $dx = 0.156$ *a.u.*. The number of time grid points is 8192, and the corresponding time step size is about $dt = 0.215$ *a.u.*. By setting both the number of spatial grid points and the number of time grid points to 16384, the convergence of the time step and the spatial step was verified, shown in Fig. S3 of the *Supplementary Materials*. In order to better analyze the disorder effect of the liquid, multiple disordered chains with the number of group M are used for simulating and statistically analyzing. For each disordered chain including N bound states, each of the bound state is set as the initial state separately to solve the TDSE. The total laser-induced current is the algebraic sum of the currents along different random chains by:

$$J_{total}(t) = -\sum_{m=1}^{M}\sum_{n=1}^{N}\langle\psi_{mn}(x,t)\,|\hat{p}|\,\psi_{mn}(x,t)\rangle\,. \tag{4}$$

Harmonic spectrum can be simulated by

$$P \propto \left|\int J_{total}(t)e^{-i\omega t}dt\right|^2. \tag{5}$$

3. Results and discussion

High-order harmonic spectra from liquid systems with different values of σ are simulated. As shown in Fig. 2(a), for the case of $\sigma = 1.0$, only odd-order harmonics are present in the high-order harmonic spectrum and there is a distinct plateau structure with the corresponding cutoff energy is at the 19^{th} order. There are still clear harmonic orders after the cutoff with the maximum photon energy is at the 35^{th} order. To distinguish between these two energy values, the maximum harmonic energy resolved in the spectra is defined as Ω_m, and the cutoff energy of the plateau is defined as Ω_c. The value of Ω_m is consistent with the discussion shown in Ref. [22]. Spectral minima tend to appear in the liquid harmonic spectrum, where the intensity of certain harmonic orders is significantly weaker than that of their adjacent orders, such as the 7^{th} and 15^{th} orders. As the degree of disorder is varied, the plateau structure remains in the spectrum for $\sigma = 1.3$ and 1.5. The maximum photon energy of the harmonic changes to the 29^{th} and 23^{rd} orders, while the cutoff of the plateau is almost unchanged. This behavior is consistent with the discussion in Ref. [30]. Those results confirm the dependence of the harmonic cutoff on the disorder degree in liquid. In order to verify the robustness of the interference minimum phenomenon, high-order harmonics are also calculated for the cases of $\sigma = 0.1, 0.5$, and 0.9, as shown in Fig. 2(b). The intensity of the 15^{th} harmonics is also weaker than both the 13^{th} and 17^{th} order harmonics. The harmonic spectra generated under different laser field parameters (*e.g.,* $E_2 = 0.2E_1$ and $0.4E_1$) are also simulated. The results indicate that this minimum phenomenon still exists, see Fig. S6 of the *Supplementary Materials*. This rules out the possibility that this minimum is caused by specific laser field parameters. The tests for the convergence of the simulation results with respect to other parameters can be found in Fig. S3-S5 of the *Supplementary Materials*. This indicates that the spectral minimum phenomenon is not an accidental numerical result and may involve the mechanism of liquid harmonic radiation. Due to the 15^{th} order harmonic is completely suppressed due to destructive interference for the case of $\sigma = 1.5$. We take the case $\sigma = 1.5$ as an example in the following discussion to investigate the physical mechanism of the minimum phenomenon in the harmonic spectrum.

To investigate the reason of destructive interference in the 15^{th} order harmonic, the interband and intraband harmonic spectra are calculated by superimposing $M = 10$ atomic chains, each containing $N = 128$ atoms, as

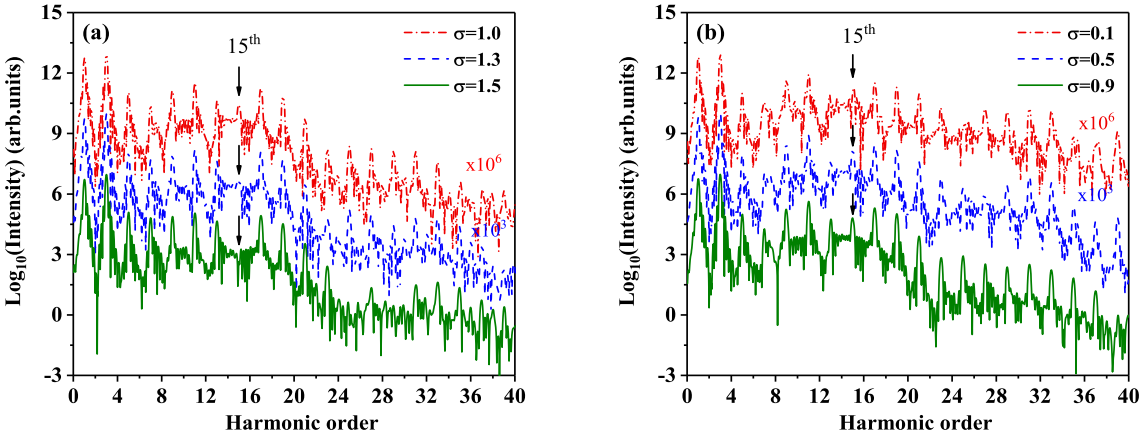


Fig. 2. High-order harmonic spectra calculated from liquid systems with different degrees of disorder.(a) for the cases of $\sigma = 1.0, 1.3$ and 1.5, (b) for the cases of $\sigma = 0.1, 0.5$, and 0.9, respectively.

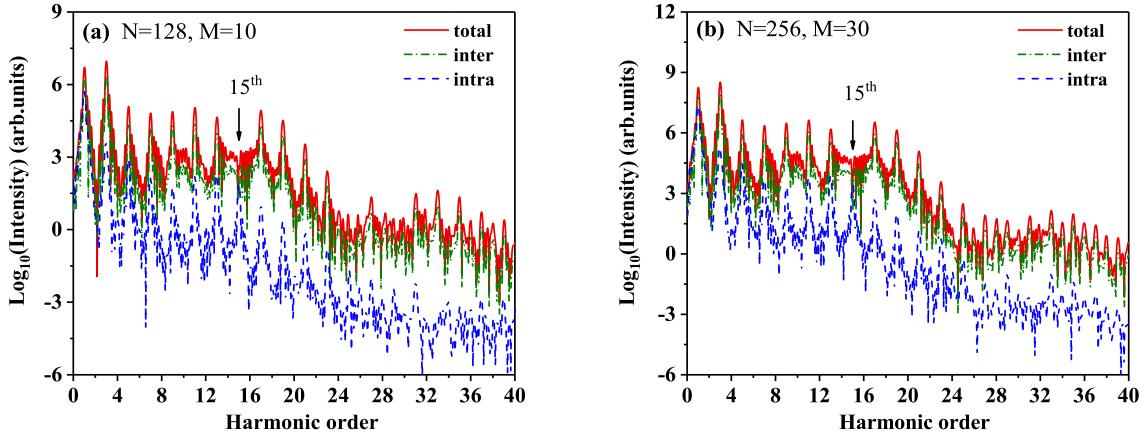


Fig. 3. Interband and intraband harmonic spectra from liquids. The statistical parameters of the random model system are (a) $N = 128$ and $M = 10$, (b) $N = 256$ and $M = 30$. The laser parameters are identical to those in Fig. 2.

shown in Fig. 3(a). The intraband harmonic spectrum primarily contributes to the low-order harmonics, while its intensity decreases sharply with increasing harmonic orders. The intensity of the interband spectrum is two to three orders of magnitude higher than the intraband spectrum above the 7^{th} order harmonic. Although the intraband spectrum can emit the 15^{th} order harmonic, the intensity is still weaker than the interband intensity. This suggests that harmonics in the plateau region originate from the interband transition processes. To check whether the feature is robust, we also simulate a larger number of atomic chains with greater length to verify the phenomenon. Fig. 3(b) calculates the intraband and interband harmonic spectra using a configuration of 30 chains, and each chain consists of 256 atoms. The results for this configuration are in agreement with those in Fig. 3(a). To verify the convergence of the results, we also simulate the harmonic spectra when $N = 128$ and M is $1, 5$, or 30. The results which are shown in Fig. S4 of the *Supplementary Materials* are consistent with those in Fig. 3(a) and Fig. 3(b). This method of statistically analyzing multiple configurations can also be referred to in reference [24]. Hence, the destructive interference at the 15^{th} order harmonic originates from the interband transition processes, and this might imply the specific physical mechanism of liquid HHG.

Because the interband harmonics are generated by the eletronic transitions of electrons from the quasi-free states back to the bound states, we simulate the TDPI of quasi-free states. As shown in Fig. 4(a), the electrons

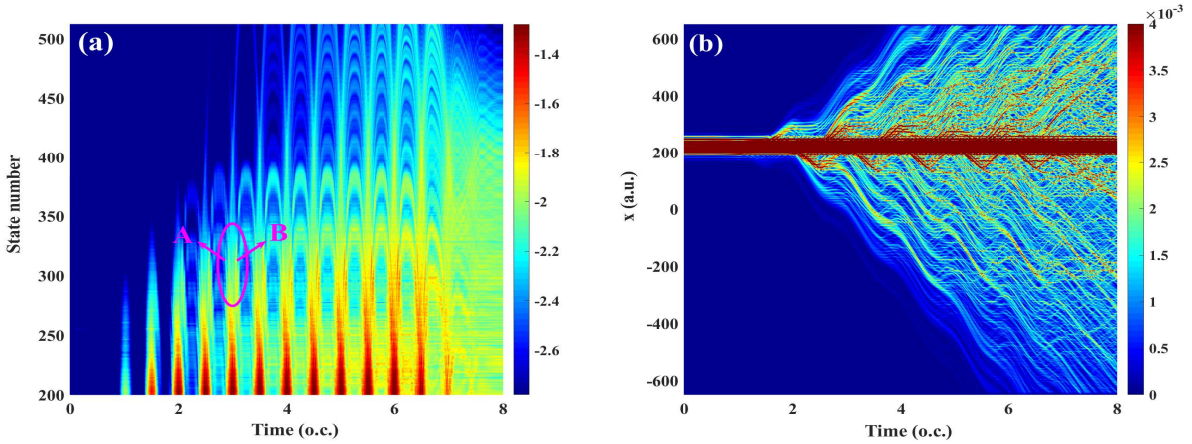


Fig. 4. (a) TDPI of quasi-free states. (b) The time-dependent probability evolution of electrons in the coordinate space from the initial state of $\phi_{125}(x)$.

in the bound states are excited to the quasi-free states under the action of the laser. In the quasi-free states, they can be further excited to the state $\phi_{378}(x)$, the energy difference $\Delta E = E_{378} - E_{128}$ is corresponding to the cutoff position of the 19^{th} order. The population of higher states becomes weaker and the channels become more complex and this region contributes to harmonics greater than the 19^{th} order. Split peaks appear near the state $\phi_{320}(x)$ after $t = 3.0$ *o.c.*, The energy difference $\Delta E = E_{320} - E_{128}$ corresponds to the 15^{th} harmonic order. These peaks are labeled A and B with magenta circles in Fig. 4(a). This indicates that the 15^{th} order harmonic at the spectral minimum originates from the interference of different paths. The evolution of the electronic wave packet over time has been simulated to find the source of the interference paths. As shown in Fig. 4(b), take the initial state $\phi_{125}(x)$ as an example, the electrons are initially localized around the spatial region [190, 255] *a.u.*, the electron population begin to emerge in neighboring states at the time $t = 2.0$ *o.c.*, and the population becomes particularly pronounced between $t = 3.0$ *o.c.* and $t = 7.0$ *o.c.*. This indicates that electrons with local characteristics can spread to the vicinity of more distant atomic nuclei under the action of an external laser field. In this process, electrons in the bound states have a finite probability of transitioning to quasi-free states from the perspective of the energy representation and can acquire higher energy. The electrons have the opportunity to return to the position of the initial localized state of the nucleus for each random atomic chain during the subsequent evolutionary process, *i.e.*, $\phi_4(x)$ or $\phi_{125}(x)$ as in this example, and also have the opportunity to transition to other localized states of the surrounding nuclei on the bound states, thereby contributing to harmonic emission.

To separate the contribution of HHG from those two parts, we define the current $J_{I(II)}(t)$ as:

$$J_{I(II)}(t) = -\sum_{m=1}^{M}\sum_{n=1}^{N}\left\langle \Phi_{mn}^{I(II)}(x,t)\,|\hat{p}|\,\psi_{mn}^{q}(x,t)\right\rangle + c.c., \tag{6}$$

where $J_I(t)$ represents the induced current generated when electrons return to the position corresponding to the initial localized state, and

$$|\Phi_{mn}^{I}(x,t)\rangle = \sum_{i=n,\ N-n+1} |\phi_{m,i}(x)\rangle\langle\phi_{m,i}(x)|\psi_{mn}(x,t)\rangle. \tag{7}$$

$J_{II}(t)$ represents the induced current generated when electrons return to other bound states surrounding the

initial localized state, and

$$|\Phi_{mn}^{II}(x,t)\rangle = \sum_{i\ (i\neq n,\ N-n+1)} |\phi_{m,i}(x)\rangle\langle\phi_{m,i}(x)|\psi_{mn}(x,t)\rangle. \tag{8}$$

In the calculation, $\phi_{m,n}(x)$ is the $n-th$ bound state in the $m-th$ group of random chain. $\psi_{mn}(x,t)$ is the time-dependent wave function obtained by evolving the initial state $\phi_{m,n}(x)$. $\psi_{mn}^{q}(x,t)$ is the distribution of the time-dependent wave function on the quasi-free state. $\phi_{m,N-n+1}(x)$ and $\phi_{m,n}(x)$ are a pair of resonant states in this model. Equation (6) shows that $J_{I(II)}(t)$ is calculated by summing up all the cases of the initial states (N bound states in each chain) of M sets of chains. In our simulations, the current $J_I(t)$ can be further separated into $J_{IA}(t)$ and $J_{IB}(t)$, corresponding to transitions returning to the initial state $\phi_n(x)$ and the corresponding resonant state $\phi_{N-n+1}(x)$, respectively. The harmonic contribution from the currents $J_{IA}(t)$, $J_{IB}(t)$, $J_I(t)$ and $J_{II}(t)$ are defined as path IA, path IB, path I, and path II, and path I is the sum of the contributions of path IA and path IB. The schematic diagrams of these transition paths are shown in Fig. 1(d), and it can be seen that the interband harmonic is equivalent to the contribution of path IA, path IB and path II, see the discussion in Fig. S8 of the *Supplementary Materials*. This decomposition of the harmonic path holds only in the regime where the contribution of transitions to states far from the initial state is negligible. The harmonic spectra from those two paths are simulated as shown in Fig. 5(a), the intensities of HHG from the path I and path II are overall comparable, while both display a pronounced minimum at the 15^{th} order. The probability of electrons returning to the spatially localized position of the initial state is greater than that of returning to other states, yet the number of other states is much larger and this led to the harmonic intensities from the two paths being approximately equal. Through simulation, it is found that when electrons return to other states, the 15^{th} order harmonic is rarely generated under this condition. However, when counting the number of electronic transitions back to the initial state in each random atomic chain, a stronger 15^{th} order harmonic radiation can be observed. As shown in Fig. 5(b), clear odd-order harmonics are obtained by counting the harmonic radiation from the transition to each initial state for those random chains, which is labeled path IA in Fig. 5(b) by a solid red line. Meanwhile, when the electrons return to the resonant state corresponding to the initial state after undergoing an electronic transition, harmonics with comparable intensity are also obtained, which is labeled path IB in Fig. 5(b) by a dashed black line. The intensities of the 15^{th} order harmonic are comparable for both paths. The 15^{th} order harmonic from path IA and path IB must have undergone destructive interference to be consistent with the situation shown in Fig. 5(a) where path I does not have the 15^{th} harmonic radiation.

To confirm this point, the phase difference of harmonic from path IA and path IB is calculated. The phase of a harmonic component is $\varphi_{IA(B)} = arg[J_{IA(B)}(\omega)]$, and $J_{IA(B)}(\omega) = \int J_{IA(B)}(t)e^{-i\omega t}dt$ is the Fourier transform of the induced current. The phase difference between the contribution of path IA and path IB is calculated by $\Delta\varphi = \varphi_{IB} - \varphi_{IA}$. The harmonics in liquids arise from the collective response of disordered systems. Therefore, the phase differences are calculated by summing over $N = 128$ initial states and $M = 10$ sets of random chains. As shown in Fig. 5(d), the absolute values of the phase differences of most harmonics are below 0.2π, and their contributions interfere constructively with the total harmonic emission. The phase differences of the other several harmonics are relatively scattered, but only the 15^{th} order harmonic has a phase difference -0.95π, which is nearly equal to $-\pi$, causing the 15^{th} harmonic to interfere destructively. This well explains the reason why the 15^{th} order harmonic is not radiated in the total harmonic. The phase difference

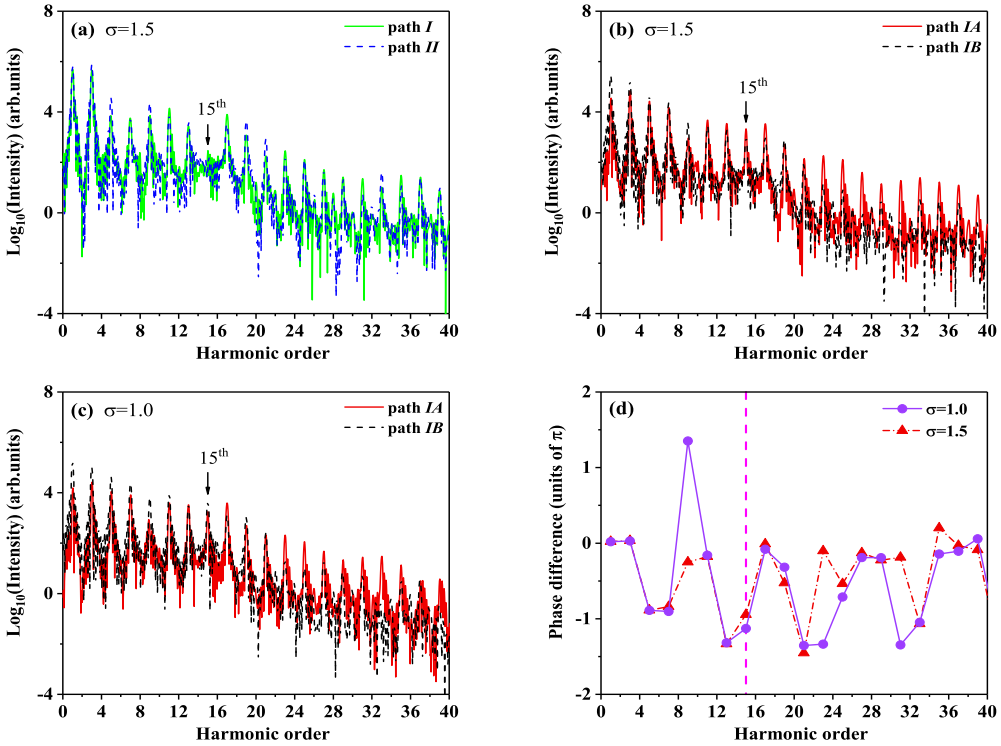


Fig. 5. (a)-(b) HHG generated from path I, path II, path IA and path IB for the case of $\sigma = 1.5$. (c) HHG generated from path IA and path IB for $\sigma = 1.0$. (d) The phase difference between path IA and path IB for $\sigma = 1.0$ and 1.5.

can be directly demonstrated in complex harmonic amplitudes, see Fig. S9 of the *Supplementary Materials*. To further verify the robustness, we also simulated the HHG under other parameters, Fig. 5(c) shows the harmonic spectra contributed from the path IA and path IB for the case of $\sigma = 1.0$. The 15^{th} order harmonics with comparable radiation intensities appeared for both paths, while the $15th$ order harmonic is actually a very small value in the total harmonic spectrum shown in the Fig. 2(b). The phase differences of harmonic from path IA and path IB for the case of $\sigma = 1.0$ are also simulated in Fig. 5(d), and the phase difference of the 15^{th} order harmonic is still close to $-\pi$ just as expected. Overall, electrons excited to the quasi-free states by the laser pulse may return to various bound states and radiate harmonics. The symmetries of the resonant states on the bound states are different, which can lead to different phases of the paths contributing to the harmonics. By separating the recombination paths, we found that the main reason for the appearance of an interference minimum in the total harmonics is that the interference of path IA and path IB are destructive.

In order to further verify the mechanism of the interference destructive phenomenon, harmonics in liquid systems from different wavelengths of laser pulse are simulated. Since the energy of photons of different wavelengths is different, the horizontal axis is set in eV as the unit to better compare the position pattern of the spectral minimums of harmonic interference, as shown in Fig. 6(a)-(d). The minimum energy of HHG are 8.59 eV, 9.75 eV, 10.75 eV, and 12.41 eV, for the case of $\lambda_1 = 1300$ nm, 1400 nm, 1500 nm and 1700 nm, respectively. In addition, the minimum of the 15^{th} order is corresponding to 11.63 eV for the case of $\lambda_1 = 1600$ nm, as shown in Fig. 2. Obviously, the position of the interference minimum increases as the wavelength increases. To visually illustrate the pattern, Fig. 6(e) shows the position of the spectral minimum changing with the laser wavelength, and the spectral minimum increases approximately linearly with the wavelength of the fundamental laser. The least squares method is used to fit the relationship between the position of the spectral minimum and

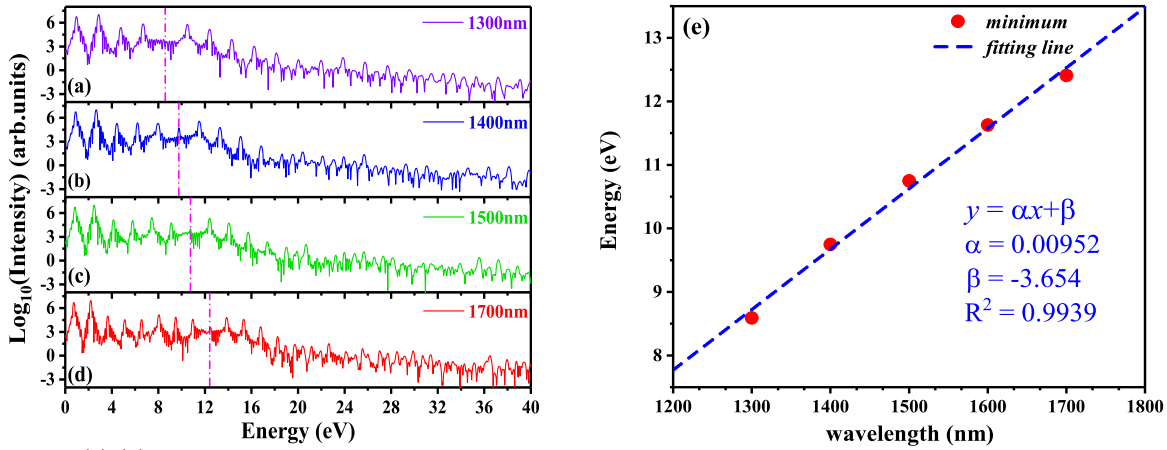


Fig. 6. (a)-(d) Harmonic spectra under different wavelengths of the fundamental laser field $\lambda_1 = 1300\ nm$, $1400\ nm$, $1500\ nm$, and $1700\ nm$. The magenta dotted dashed lines represent the position of the minimum harmonic energy. (e) The dependence of the energy minimum on the wavelength of the fundamental laser field.

the wavelength. By using eV and nm as units of the position of the minimum and the wavelength respectively, the parameters are $\alpha = 0.00952$ and $\beta = -3.654$ for the fitting formula $y = \alpha x + \beta$. And the coefficient of determination of the fit is $R^2 = 0.9939$, which is very close to 1. Further simulations show that the empirical formula does not extrapolate well; that is, its applicability is limited to the range of 1300-1700 nm. The results can be seen in Fig. S7 of the *Supplementary Materials*. For shorter wavelengths, such as 1200 nm, the energy of spectrum minimum is close to band gap of the system. Harmonics generation may not only come from interband harmonic, but also from intraband harmonic. This is beyond the scope of the discussion in this paper, which is about the spectral minimum caused by interband harmonics. For longer wavelengths, such as 1800 nm, the intensity of the 19^{th} order harmonic in the simulation results is weaker than that of the adjacent harmonic orders. Although it is qualitatively consistent with the prediction of this empirical formula, the harmonics at 19^{th} order still persist and have not dissipated. For the case of 2000 nm. There are three harmonic minima, *i.e.,* 15^{th}, 21^{st} and 25^{th}. This indicates that the liquid harmonic interference channel driven by long wavelengths is more complex, and our empirical formula cannot explain all cases. We attribute this phenomenon to the fact that, when driven by longer-wavelength lasers, electrons have the opportunity to move closer to atoms whose positions are farther away from the localization initial states. The vibration period is also longer, allowing electrons to obtain greater energy. Thus, when they return to the initial state or the corresponding resonant state, they acquire higher energy, leading to an increase in the minimum position with increasing wavelength. The physical mechanism of the interference minima of harmonic orders using the conclusion presented in Fig. 5 is verified. We find that it is in good agreement with the interference minimum of harmonics in the range $[8.59, 11.63]\ eV$, except for the case of 12.41 eV,*i.e.,* the case of 1700 nm in our simulation. To find out why the above mechanism does not apply at 1700 nm, we employed a method to separate the contribution from path I and path II.

The minimum energy 12.41 eV corresponds to the 17^{th} order for the case of 1700 nm in the total harmonic spectrum. However, the 17^{th} order harmonic is no longer an interference minimum for path I or path II, as shown in Fig. 7(a), is contrast to the behavior shown in Fig. 5(a). The phase differences of the harmonics between path I and path II are calculated, as shown in Fig. 7(b). The phase difference of the 17^{th} order harmonic is 1.159π, which is nearly π and thus satisfies the interference condition. In a word, the spectral

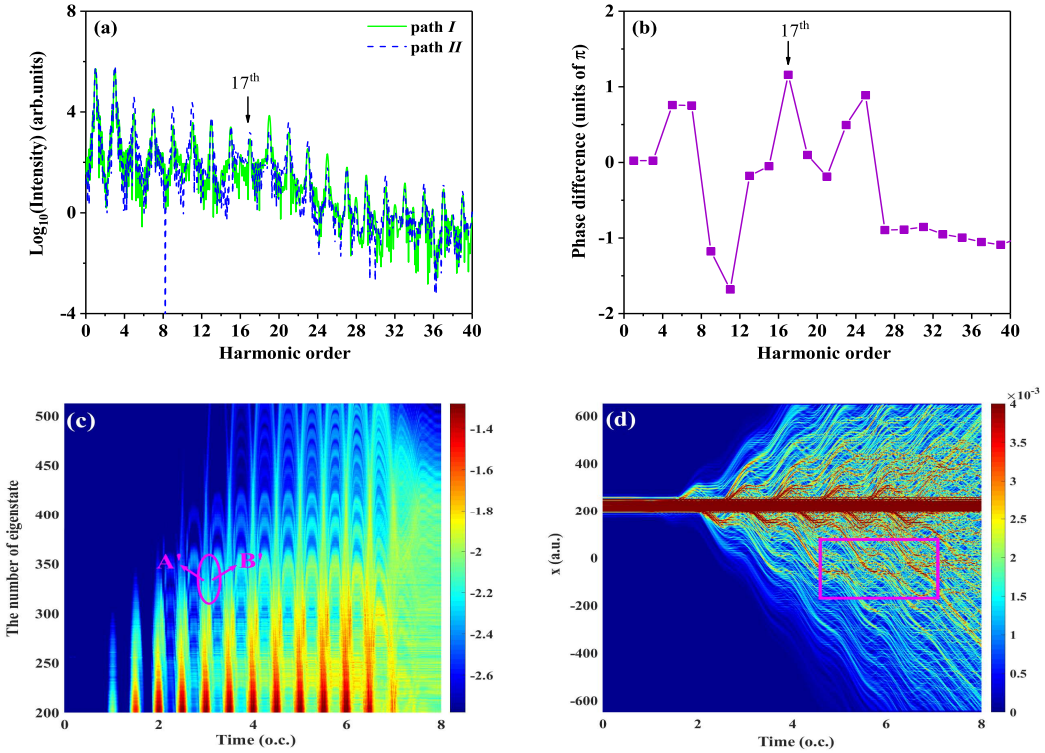


Fig. 7. (a) The harmonic spectra generated from path I and path II for the case of 1700 nm. The black arrows denote the position of the 17^{th} order harmonic. (b) The phase difference between path I and path II for $\sigma = 1.5$. (c) TDPI of quasi-free states. (d) The time-dependent probability evolution of electrons in the coordinate space from the initial state $\phi_{125}(x)$. The magenta rectangular boxes designate the areas distinct from those in Fig. 4.

minimum of interference in this case comes from the cancellation of interference between path I and path II, rather than between path IA and path IB. Longer wavelength laser pulses can drive electrons to move to greater distances, which can be illustrate by the population of the electron being in other eigenstates (except for initial state and the resonance state), see Fig. S10 of the *Supplementary Materials*. In contrast to previously proposed interference mechanisms in HHG [34–37], the harmonic minima in liquids are not associated with fixed spatial structural configurations or with emissions from different channels in momentum space, but rather with coherent interference among distinct recombination channels induced by localized resonant states within the disordered structure. The contribution of path II is closely related to the recently reported off-site recombination mechanism in liquid HHG [28]. In both cases, electrons are driven away from their initial localized regions and can recombine with other localized states. However, off-site recombination mainly emphasizes the spatial origin of harmonic emission and explains the formation of additional harmonic structures, whereas the path II in present work is derived from the energy representation suggesting the path for electrons to return from a quasi-free state to another bound states with energy different from the initial state. This makes the interference mechanism more complex.

Harmonics generated from other wavelengths like 1800 nm and 2000 nm, are also simulated to verify this phenomenon and the results can be seen in Fig. S7 of the *Supplementary Materials*. Although the interference path for the range of [1300, 1600] nm and the 1700 nm case are not identical, the analytical method of decomposing the contribution paths is similar. It should be noted that both the path decomposition method and the range of applicability for extrapolation of the empirical formula presented in this paper are limited to 1300-1700 nm. This is because at longer wavelengths the path becomes more complex, requiring a more detailed

decomposition of the path. We have not yet found a unified theory to explain all the cases of these minima, but the method of separating paths in this paper is instructive for the study of liquid harmonic generation. The TDPI of quasi-free states is simulated in Fig. 7(c), and their evolution over time is similar to that shown in Fig. 4(a). There are two split peaks marked by the $A^{'}$ and $B^{'}$ paths with a magenta circle near the state $\phi_{335}(x)$ after $t = 3.0$ *o.c.*. These correspond to path I and path II and are the source of the interference minimum of 17^{th} order. The time-dependence electron population is simulated to visually demonstrate the movement pattern of electrons in space, as shown in Fig. 7(d). Compared with the Fig. 4(b), the electron population is much larger for the time range from 4.5 *o.c.* to 7.0 *o.c.*, as indicated by the magenta rectangular boxes. This indicates that the total harmonics contributed by the surrounding states cannot be ignored. When the path back to the initial state position interferes with the path back to the surrounding states, *i.e.,* path I and path II, a minimum will also appear on the harmonic spectrum.

4. Conclusions

In summary, a one-dimensional random atomic chain model is used to characterize liquid systems. By numerically solving the TDSE, the high-order harmonic spectra are calculated under a two-color laser field in this paper. Liquid systems with different degrees of disorder all feature a minimum in their total harmonic spectra, which becomes more obvious as the disorder increases. For the case of $\sigma = 1.5$, the 15^{th} order harmonic is completely suppressed due to destructive interference. The minimum energy of the harmonic increases monotonically with the increase in wavelength in the range of 1300 nm to 1700 nm. Because the bound states of the liquid systems are localized and have resonant states at the same coordinate position, the current is decomposed into contributions from transition to the initial state, the resonant state of the initial state and other bound states, and define them as path IA, path IB, and path II, respectively. The sum of the contributions of path IA and path IB is defined as path I. By analyzing the contribution of these paths to the harmonics, it is found that the interference minimum of the harmonic occurs when the interference between path IA and path IB cancels out for the case of $\lambda_1 \in [1300, 1600]$ nm. Further research reveals that at 1700 nm, the harmonic minimum is not the result of the interference between path IA and path IB; instead, it is caused by the interference between path I and path II. This is because the laser with longer wavelength has a higher probability of driving electrons to more distant region, and the contribution of path II is stronger. TDPI of quasi-free states and the time-dependent probability evolution of electrons in the coordinate space are also simulated to illustrate the underlying physical processes. The one-dimensional model used in this paper has some limitations. It can only simulate the harmonic radiation under the action of linearly polarized laser, and it fails to take into account the molecular structural properties of the liquid. The structure of the ignored liquid molecules for a real three-dimensional liquid systems may also affect the interference of liquid harmonic radiation. A real liquid model should be constructed to simulate liquid HHG for future work, and the perspective presented in this paper still hold significant value for understanding the phenomenon of interference minimum and providing a research path for analyzing ultra-fast processes in liquids.

Acknowledgment

This work is supported by the National Natural Science Foundation of China (NSFC) (Grant Nos. 11504221), the Natural Science Foundation of Shanxi Province, China (Grant No. 201901D111288), the Scientific and Technological Innovation Programs of Higher Education Institutions in Shanxi, China (GrantNo. 2019L0452), and the China Postdoctoral Science Foundation (Grant No. 2020M682525).

References

[1] Hentschel R K M, Kienberger R, Reider G A, Milosevic N, Brabec T, Corkum P, Heinzmann U, Drescher M and Krausz F 2001 *Nature* **414** 509-513

[2] Paul P M, Toma E S, Breger P, Mullot G, Augé F, Balcou P, Muller H G and Agostini P 2001 *science* **292** 1689-1692

[3] Shore B W and Knight P L 1987 *J. Phys. B: At. Mol. Opt. Phys.* **20** 413

[4] Krause J L, Schafer K J and Kulander K C 1992 *Phys. Rev. Lett.* **68** 3535-3538

[5] Chin A H, Calderón O G and Kono J 2001 *Phys. Rev. Lett.* **86** 3292-3295

[6] Zhao Y, Liu Z J, Wang S, Huo X X, Xing Y H and Zhang J 2025 *Chin. Phys. B* **34** 033201

[7] Düsterer S, Schwoerer H, Ziegler W, Ziener C and Sauerbrey R 2001 *Appl. Phys. B* **73** 693-698

[8] Quéré F, Thaury C, MonotP, Dobosz S, Martin P and Geindre J P 2006 *Phys. Rev. Lett.* **96** 125004

[9] Liu J Q and Bian X B 2021 *Phys. Rev. Lett.* **127** 213901

[10] Liu J Q and Bian X B 2024 *Nat. Commun.* **15** 10856

[11] Sun H Y, He A Y, Xiao G X and Xia C L 2025 *Opt. Commun.* **591** 132135

[12] Jia G R, Chen C, Kang H X, Liu J Q, Yuan M H and Bian X B 2025 *Opt. Commun.* **582** 131670

[13] Corkum P B 1993 *Phys. Rev. Lett.* **71** 1994-1997

[14] Higuchi T, Stockman M I and Hommelhoff P 2014 *Phys. Rev. Lett.* **113** 213901

[15] Xia C L, Li Q Q, Lan Y Y and Miao X Y 2020 *Opt. Commun.* **456** 124626

[16] Zürl R, Graener H 1998 *Appl. Phys. B* **66** 213-216

[17] Flettner A, Pfeifer T, Walter D and Winterfeldt C 2003 *Appl. Phys. B* **77** 747-751

[18] DiChiara A D 2009 *Opt. Express* **17** 20959-65

[19] Kurz H G, Steingrube D S, Ristau D, Lein M and Morgner U 2013 *Phys. Rev. A* **87** 063811

[20] Madsen L B, Jensen F, Tolstikhin O I and Morishita T 2014 *Phys. Rev. A* **89** 033412

[21] Luu T T, Yin Z, Jain A, Gaumnitz T, Pertot Y, Ma J and Wörner H J 2018 *Nat. Commun.* **9** 3723

[22] Zeng A W and Bian X B 2020 *Phys. Rev. Lett* **124** 203901

[23] Yarnell J L, Katz M J, Wenzel R G and Koenig S H 1973 *Phys. Rev. A* **7** 2130-2144

[24] Xia C L, Liu J Q, Lü L J, Zeng A W, Li Z L and Bian X B 2022 *J. Phys. B: At. Mol. Opt. Phys.* **55** 045401

[25] Mondal A, Neufeld O, Yin Z, Nourbakhsh Z, Svoboda V, Rubio A, Tancogne-Dejean N and Wörner H J 2023 *Nat. Phys.* **19** 1813-1820

[26] Neufeld O, Nourbakhsh Z, Tancogne-Dejean N and Rubio A 2022 *J. Chem. Theory Comput.* **18** 4117-4126

[27] Xia C L, Li Z L, Liu J Q, Zeng A W, Lü L J and Bian X B 2022 *Phys. Rev. A* **105** 013115

[28] Mondal A, Neufeld O, Balčiūnas T, Waser B, Müller S, Rossi M, Yin Z, Rubio A, Tancogne-Dejean N and Wörner H J 2025 *Nat. Photon.* **20** 216-224

[29] Zhang P J, Perry C, Luu T T, Matselyukh D and Wörner H J 2022 *Phys. Rev. Lett.* **128** 133001

[30] Ding Z W, Wang Y B, Li Z L and Bian X B 2023 *Phys. Rev. A* **107** 013503

[31] Chen J X and Bian X B 2023 *Phys. Rev. A* **107** 043111

[32] Mondal A, Waser B, Balciunas T, Neufeld O, Yin Z, Tancogne-Dejean N, Rubio A and Wörner H J 2023 *Opt. Express* **31** 34348-34361

[33] Lein M, Hay N, Velotta R, Marangos J P and Knight P L 2002 *Phys. Rev. Lett.* **88** 183903

[34] Lein M, Hay N, Velotta R, Marangos J P and Knight P L 2002 *Phys. Rev. A* **66** 023805

[35] Cormier E, ZaLïr A, Holler M, Schapper F, Keller U, Wyatt A, Monmayrant A, Walmsley I, Auguste T and Salières P 2009 *Eur. Phys. J. Spec. Top.* **175** 191-194

[36] Zhao Y T, Xu X Q, Jiang S C, Zhao X, Chen J G and Yang Y J 2020 *Phys. Rev. A* **101** 033413

[37] Zhang L Y, Xie Z X, Wang C, Ge X L and Guo J 2024 *Chin. Phys. B.* **33** 093201

[38] Zhang C P and Miao X Y 2023 *Chin. Phys. Lett.* **40** 124201

[39] Shao T J, Lü L J, Liu J Q and Bian X B 2020 *Phys. Rev. A* **101** 053421